Ionization of His 55 at the Dimer Interface of Dynein Light-Chain LC8 Is Coupled to Dimer Dissociation[†]

Afua Nyarko,[‡] Loren Cochrun,[‡] Stephanie Norwood,[§] Nathan Pursifull,[§] Andrea Voth,[‡] and Elisar Barbar*,[‡]

Department of Biochemistry and Biophysics, Oregon State University, Corvallis, Oregon 97331, and Department of Chemistry and Biochemistry, Ohio University, Athens, Ohio 45701

Received July 1, 2005; Revised Manuscript Received August 25, 2005

ABSTRACT: LC8 is a highly conserved light-chain subunit of cytoplasmic dynein that interacts with a wide variety of cellular proteins and is presumed to play a fundamental role in dynein assembly and cargo recruitment and in the assembly of protein complexes unrelated to dynein. LC8 is a dimer at physiological pH but dissociates to a folded monomer at pH < 4.8. We have suggested that acid-induced dimer dissociation is due to protonation of His 55, which is stacked against His 55′ and completely buried in the dimer interface. In this work, we show that the pH-induced dissociation is reversible and indeed governed by the ionization state of His 55. Mutagenesis of His 55 to Lys results in a monomer in the pH range of 3−8, while the mutation to Ala results in a dimer in the same pH range. Mutations that disrupt intermolecular hydrogen bonds between Tyr 65 and Lys 44′ and His 55 and Thr 67′ do not change the association state of the dimer. Titration curves for His 55 and the two other histidines, His 72 and 68, were determined by ^{13}C-^{1}H NMR for H55K and for WT-LC8 in the monomeric and dimeric states. The pK_a values of His 72 and His 68 are 6 in the WT dimer and 6.2−6.5 in monomeric H55K, while the pK_a of His 55 is about 4.5 in the WT dimer. These results indicate that deprotonation of His 55 is linked to dimer formation and that mutation of His 55 to a small neutral residue or to a positively charged residue uncouples the protonation and dissociation processes.

Cytoplasmic dynein is a multisubunit microtubule-based molecular motor that is involved in a wide variety of fundamental intracellular functions including mitotic spindle orientation and assembly, Golgi and vesicular transport, and nuclear migration (reviewed in ref *1*). Dynein light-chain LC8,[1] a 10-kDa component of the cytoplasmic dynein complex, is highly conserved among species and has essential roles in several organisms (*2, 3*) including *Drosophila*, where null mutations are lethal (*4*). LC8 interacts with a wide array of cellular proteins such as neuronal nitric oxide synthase, myosin V, the proapoptotic factor Bim, transcriptional factors Swallow and TRPS1, several virus proteins, p21-activated kinase 1, and p53-binding protein 1 (*5−14*). Because it binds to many unrelated proteins presumed to be dynein cargo, LC8 appears to function as a versatile adapter that links cargo proteins to the dynein motor (*5, 15*). There are also suggestions that it plays a similar role as "molecular glue" in multiprotein complexes unrelated to dynein (*16, 17*). Within the dynein complex, LC8 may initiate complex assembly by promoting an increase in structure, stability, and dimerization of dynein intermediate chain, IC74. This hypothesis is based on *in vitro* studies with a recombinant N-terminal domain of IC74 that gains secondary and tertiary structure upon LC8 binding (*18−20*). Similarly, LC8 binds the Swallow protein and promotes its assembly from a partially folded monomer to a dimer with features of a coiled coil (*21*). The ability of LC8 to promote structure formation is likely to be a general characteristic of its interactions and may enable it to perform its diverse roles in the cell. The dimeric nature of LC8 with dual symmetric binding sites for many ligands (*15, 22, 23*) could be an essential factor in bringing its interacting partners in close proximity and thereby promoting their dimerization or assembly (*21*).

The LC8 interactions characterized thus far demonstrate that LC8 functions as a dimer (*15, 22, 23*). In solution, LC8 is a moderately tight dimer at physiological pH (*24*). The crystal structure of the human dimer suggests that it is stabilized by several intermolecular hydrogen bonds including Tyr 65−Lys 44′ and Thr 67−His 55′ and by hydrophobic interactions between residues including Ile 57/57′, Phe 62/62′, Val 66/66′, His 55/55′, and Phe 86/86′. In solution, LC8 dissociates to a folded monomer at low pH (titration midpoint of 4.8) and at a low protein concentration (K_d of 12 μM) (*24*). With this high dissociation constant, it is possible that, in the cell, the local protein concentration may be sufficiently low to promote LC8 dissociation. Under such conditions,
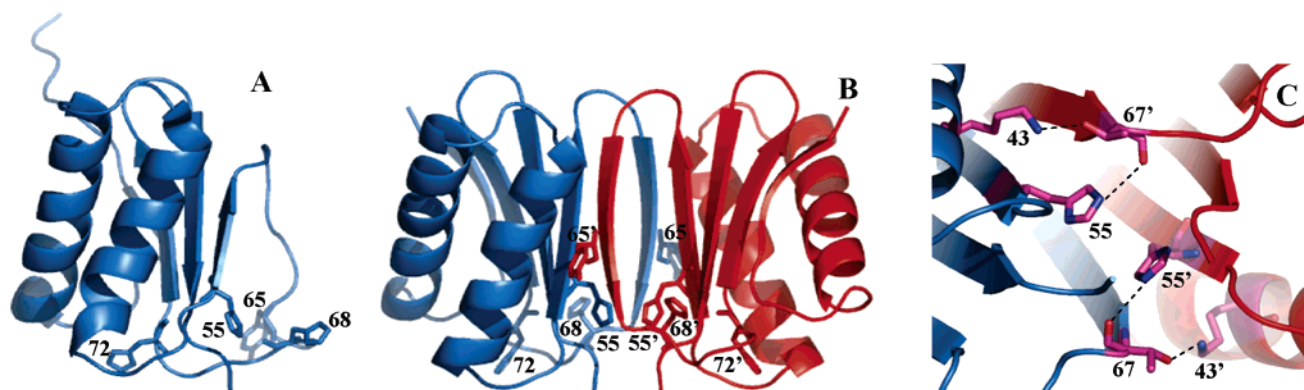
FIGURE 1: Ribbon diagram of LC8 with side chains of the three histidines and Tyr 65 in (A) the NMR structure of the pH-induced monomer of *Drosophila* LC8 and (B) the X-ray crystal structure of PIN (human LC8) dimer. The imidazole rings of 55 and 55′ at the dimer interface are 5.7 Å apart, while 68−68′ and 72−72′ are considerably exposed and distant from each other. The three histidines are all solvent-exposed in the monomer. (C) Close up view of the environment of His 55 in the human dimer, showing His 55/His 55′ stacking and hydrogen bonds between His 55 and Thr 67′ and between Lys 43 and Thr 67′. The images were produced with PyMol (Delano Scientific LLC) (*40*), using PDB code 1RHW for the monomer (*25*) and PDB code 1CMI for the dimer (*23*) (shown in this drawing without the 13-residue-bound nNOS peptide).

the monomer−dimer equilibrium could play a regulatory role in LC8 function.

Figure 1 shows a comparison of the *Drosophila* pH 3 monomeric solution structure (*25*) with the human dimeric crystal structure (*23*) and a close up view of the environment of His 55 in the human dimer. The solution structure of the monomeric protein is similar to the dimer subunit, except for an interface β strand that is somewhat disordered in the pH 3 monomer (*25*). By examination of the human dimer interface, the most likely candidate for a titrating group linked to pH-dependent dissociation is the buried histidine at position 55 (*24, 25*). His 55 is packed within 6 Å of His 55′, and their protonation would place two charged imidazole rings in close proximity in a hydrophobic environment. This energetically unfavorable situation is relieved by dissociation to the monomer and exposure of His 55 to the solvent. If protonation of His 55 is primarily responsible for the pH-dependent dimer dissociation, the pK_a of His 55 should be 4.8 in accordance with the pH midpoint of dimer dissociation determined from sedimentation equilibrium.

In this work, we report that the pH-induced dissociation is reversible in the pH range of 3−8. Titration curves of His 55 and the two other histidines in the monomer and dimer forms indicate that the ionization state of His 55 is tightly coupled to LC8 dimerization. Mutagenesis studies demonstrate that the hydrogen bonds involving the Tyr 65 side chain are not essential for the assembly of the dimer and that mutation of His 55 to Lys, which introduces a positive side chain at the interface, is sufficient to dissociate the dimer at physiological pH.

MATERIALS AND METHODS

Protein Preparation. Uniformly ^{15}N and ^{15}N/^{13}C isotopically labeled LC8 were prepared following methods described earlier (*25*). Site-directed mutagenesis was done following the GeneEditor *in vitro* protocol (Promega) using the mutagenesis oligonucleotides 5′-C AAT CCC ACA TGG AAA TGC ATT GTC GGT C-3′ for histidine (CAT) at position 55 to lysine (AAA), 5′-C AAT CCC ACA TGG GCT TGC ATT GTC GGT C-3′ for histidine (CAT) at position 55 to alanine (GCT), 5′-AAC TTT GGA TCG AAA GTC ACA CAC GAG-3′ for tyrosine (TAT) at position 65

to lysine (AAA), and 5′-C TTT GGA TCG TTT GTC ACA CAC G-3′ for tyrosine (TAT) at position 65 to phenylalanine (TTT). The mutant DNA was verified by sequencing before transformation into BL21-DE3 cell lines for protein expression. All NMR spectra were collected on 0.4−1 mM LC8 protein samples in either 50 mM sodium phosphate (pH ≥ 6.0) or 50 mM citrate phosphate (pH < 6), 50 mM NaCl, 5 mM dithiothreitol (DTT), 10% D_2O, 1 mM sodium azide, and a protease inhibitor cocktail (Roche). Purity of >95% was verified by SDS−PAGE and analytical size-exclusion chromatography.

Hydrodynamic Measurements. The molecular masses of the proteins were determined by analytical ultracentrifugation and size-exclusion chromatography. Ultracentrifugation experiments were performed at 4 °C with a Beckman Optima XL-A ultracentrifuge. Three protein concentrations 75, 37.5, and 18.7 μM in 50 mM sodium phosphate, 50 mM NaCl, and 0.5 mM sodium azide at pH 7.8 were analyzed at rotor speeds of 40 000 and 28 000 rpm. Size-exclusion chromatography experiments were done using a TSK2000SW (TosoHaas) HPLC column (7.8 mm × 60 cm, particle size of 5 μm) at a flow rate of 0.5 mL/min. The running buffer was 50 mM sodium phosphate at pH 7.3 or 50 mM citrate phosphate at pH 3 with 0.2 M sodium sulfate, 5 mM DTT, and 1 mM sodium azide. Proteins were detected by their absorbance at 280 nm. The association states were determined using a multi-angle light-scattering instrument (mini-DAWN, Wyatt Technology), which was placed in line with UV and refractive index detectors during size-exclusion chromatography.

NMR Spectroscopy. All NMR spectra were collected at 25 °C on a 600 MHz Bruker DRX spectrometer. Spectra were processed with NMRPipe (*26*) and analyzed with NMRView (*27*). Two-dimensional [1]H-^{15}N heteronuclear single-quantum correlation (HSQC) experiments were recorded using States-TPPI phase discrimination of 256 increments defined by 128 scans and 1024 points. Constant-time HSQC spectra (*28*) collected in the aromatic region were recorded with 1024 and 256 complex points in the ^{1}H and ^{13}C dimensions, respectively. [1]H chemical shifts were referenced with internal 2,2-dimethylsilapentene-5-sulfonic acid (DSS) at 0 ppm. The pH of each sample was measured

before and after each experiment, and the average reading was used for data analysis.

Data Analysis. The pH titration data were analyzed by nonlinear least-squares fit to a monophasic model using eq 1, which is derived from simple acid dissociation equilibrium for titration of one group and assumes no interaction with neighboring groups, and a rapid equilibrium between protonated and unprotonated forms

$$\delta_{\mathrm{obs}} = \frac{\delta_{\mathrm{HA}} + \delta_{\mathrm{A}^-} \times 10^{(\mathrm{pH}-\mathrm{p}K_a)}}{1 + 10^{(\mathrm{pH}-\mathrm{p}K_a)}} \qquad (1)$$

where δ_{HA} is the chemical shift in the acidic pH limit and δ_{A^-} is the chemical shift in the basic pH limit for both the ^{1}H and ^{13}C resonances. A single resonance is observed for histidines of the same residue in both subunits in the symmetrical dimer and is in slow exchange with the resonance corresponding to the same residue in the monomer. Because all titration data fit well to a simple model with a single inflection, no attempt was made to fit the data to a more complex model.

RESULTS

Interface Mutants of LC8. Among the hydrogen bonds that in the crystal structure appear to stabilize the dimer interface are those formed between phenolic OH of Tyr 65 and the side chain Nϵ of Lys 44′ and between NϵH of His 55 and the backbone C=O of Thr 67′. Replacement of Tyr 65 with Phe and with Lys results in stable dimers at pH 7 similar to WT-LC8 (Figure 2A). The elution profile of Y65F is identical with that of WT-LC8, but Y65K elutes slightly earlier. The earlier elution of Y65K is possibly due to a local expansion in the dimeric structure but is not due to global unfolding because far-UV CD spectra (molar ellipticity) are similar to the WT (data not shown). The molecular weights determined from on-line multi-angle light scattering confirmed the dimeric states of Y65K and Y65F and the monomeric state of H55K discussed later and shown here for comparison.

If protonation of His 55 causes dissociation, then mutation of His 55 to Lys is expected to result in a monomer at pH 7, while a mutation of His 55 to Ala is expected to result in a dimer at all pH values at which the protein is still folded. Mutation of His 55 to Ala will eliminate the His 55 NϵH hydrogen bond with the backbone C=O of Thr 67′. H55A has a size-exclusion elution profile similar to WT-LC8, an indication that H55A is a dimer, as predicted, while H55K has an elution profile consistent with a monomer (Figure 2B). Analytical ultracentrifugation experiments confirm that H55K is a monomer at pH 7 with no detectable dimeric population. At 75 μM, a mass of 10 369 D was obtained by sedimentation equilibrium (the monomeric protein has a theoretical mass of 10 365 D).

Acid-Induced Dimer Dissociation of LC8 Is Reversible. Size-exclusion chromatograms of WT-LC8 at pH 7 and 3 and at pH 7 after incubation at pH 3 are shown in Figure 2C. The protein elutes later at pH 3 than at pH 7, as expected for a protein of smaller size. The pH 7 peak obtained after incubation of the sample at pH 3 (pH 7*) superimposes on the pH 7 peak for the sample maintained at pH 7. This demonstrates that pH dissociation is reversible. Additional
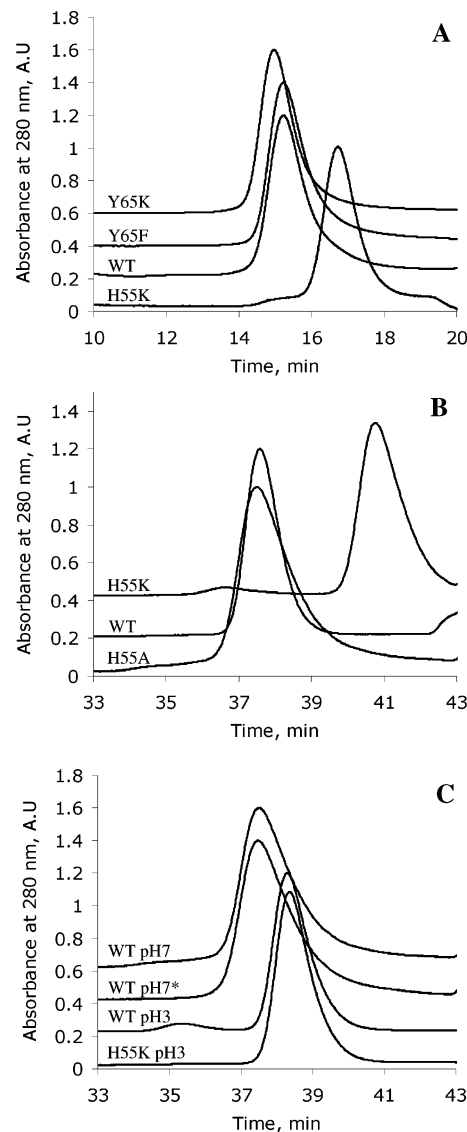

FIGURE 2: Association state(s) of WT-LC8 and LC8 mutants. (A) Size-exclusion chromatograms of Tyr 65 mutants of LC8 at pH 7. Y65F and Y65K are both dimeric. WT-LC8 and monomeric H55K are shown for comparison. All proteins in this experiment retained the His-tag fusion peptide. Experiments were done at a flow rate of 0.8 mL/min on a Superdex 75 column, using protein concentrations of 20 μM and a running buffer of 50 mM sodium phosphate, 0.2 M sodium sulfate, and 5 mM DTT. (B) Elution profiles of WT-LC8, H55A, and H55K at pH 7. H55A is a dimer at pH 7, while H55K is a monomer. (C) Elution profiles of WT-LC8 at pH 7, WT-LC8 at pH 3, and WT-LC8 at pH 7 after incubation at pH 3 shown as pH 7*. The pH-induced monomer associates to form a dimer when the pH is raised back to 7. H55K at pH 3 is shown for comparison. For B and C, experiments were done on the proteins without the His tag at a flow rate of 0.5 mL/min on a TSK2000SW (TosoHaas) HPLC column, using protein concentrations of 25 μM and a running buffer of 50 mM sodium phosphate, 0.2 M sodium sulfate, and 5 mM DTT for pH 7 or 50 mM sodium citrate, 0.2 M sodium sulfate, and 5 mM DTT for pH 3.

evidence for reversibility is obtained from ^{1}H-^{15}N HSQC spectra in which peaks observed at pH 7 and 3 have considerable differences in chemical shift, but peaks of the sample that has been incubated at pH 3 then dialyzed back to pH 7 are superimposable on peaks of the sample maintained at pH 7 (data not shown).

The pH-induced WT monomer elutes earlier than monomeric H55K at pH 7, suggesting that the protein is somewhat
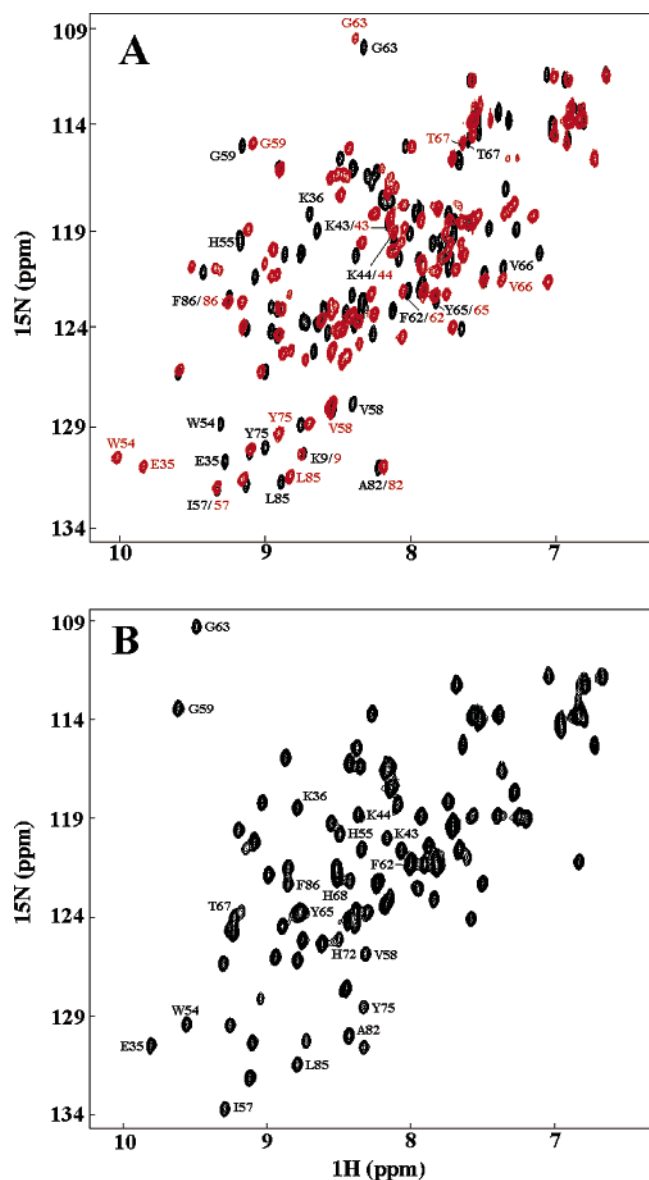
FIGURE 3: ^{15}N-^{1}H HSQC spectra of (A) WT-LC8 at pH 3 (black) and H55K at pH 7 (red) and (B) WT-LC8 at pH 7. The assignments of residues at the interface and other representative residues are shown. Spectra were recorded on a Bruker DMX 600 spectrometer using protein concentrations of ~500 μM in 50 mM sodium citrate or sodium phosphate buffer.

expanded at pH 3. This expansion is consistent with the increase in local disorder observed in the NMR structure at pH 3 (*25*). H55K at pH 3 migrates similar to the WT at pH 3 (Figure 2C), indicating that the slow migration is a low pH effect, perhaps associated with the local expansion of the protein and not due to a subpopulation of dimers. H55K and WT-LC8 at low pH are folded because they have similar molar ellipticity in far-UV CD spectra as the pH 7 sample (*24*; data not shown). Similar size-exclusion elution profiles obtained for H55A at pH 7 and 3 confirm that H55A remains a folded dimer at low pH.

NMR Characterization. The ^{1}H-^{15}N HSQC spectrum of monomeric H55K at pH 7 was compared to that of monomeric WT-LC8 at pH 3 to assess their similarity in average overall structure (Figure 3A). Peak dispersion in the amide region and the similarity in chemical shift of interface residues (Y65 and I57, for example) and noninterface residues (A82 and K9, for example) show that H55K is a

folded monomer similar to the pH-induced WT monomer. The few differences in chemical shift between H55K at pH 7 and WT at pH 3 are due to the proximity to the mutation site (W54) and to the difference in pH (E35 is titrated between pH 3 and 7) and are consistent with changes associated with the local expansion of the protein at pH 3 as inferred from size-exclusion chromatography. NMR spectra of H55K at pH 7 and WT monomer at pH 3 are considerably different from spectra of the WT dimer at pH 7 (Figure 3B), specifically at interface residues (Y65, G63, G59, I57, and H55, for example). ^{1}H-^{15}N HSQC spectra for H55A are similar to dimeric WT-LC8 at pH 7 (data not shown), consistent with H55A being a folded dimer.

Heteronuclear NMR spectroscopy is ideally suited for determination of residue-specific pK_a values in proteins (*29–33*). The C2H chemical shifts of imidazole side chains are considerably downfield-shifted and remote from the rest of the aromatic resonances and therefore easily assigned in ^{13}C-^{1}H HSQC spectra. Figure 4 shows ^{13}C constant-time HSQC spectra corresponding to the C2H resonances of histidine residues for H55K (A), WT-LC8 (B), and H55A (C). Each spectrum is an overlay of data collected at pH 3 (black), pH 5 (blue), and pH 7 (red). At pH 3, three peaks corresponding to His 55, His 68, and His 72, assigned according to ref *25*, are observed for WT-LC8 in the monomeric form (B, black). As expected at pH 3, only the two C2H peaks corresponding to His 68 and His 72 are observed for H55K (A) and H55A (C), and they shift downfield as the pH is increased from 3 to 8. The three C2H histidine peaks in WT-LC8 are also shifted downfield as the pH is increased, but unlike the mutants, peaks corresponding to both the monomer (labeled m) and dimer (labeled d) are observed at pH 5. The presence of two C2H peaks for each His residue at intermediate pH (from 4.2 to 5.3) indicates that the monomer–dimer equilibrium is slow on the NMR time scale, giving rise to one peak for the monomer and one peak for the dimer for the same C2H. His 72 and His 68 in the WT-LC8 dimer were assigned by comparison of their chemical shifts with the corresponding resonances in the His 55 mutant dimer (H55A). His 55 C2H in the WT dimer was assigned to the most downfield peak in the ^{13}C dimension (chemical shift of 137.8 ppm) that is only present in the WT dimer. Interestingly, there is no chemical-shift change in the peak corresponding to His 55 dimer (55d) between pH 5 (Figure 4B, blue) and pH 7 (Figure 4B, red), indicating that His 55 is already titrated to a neutral form in the dimer. The large difference in chemical shift between His 55 and the other histidines in the dimer is attributed to the aromatic–aromatic stacking of His 55 with His 55′ at the interface and to its deprotonation at pH 5, while the other histidines are still protonated at this pH.

pH Titrations of Histidine Residues in WT-LC8. The ^{13}C and ^{1}H chemical shifts for WT-LC8 were plotted as a function of pH (Figure 5). Parts A and C of Figure 5 show proton and carbon chemical-shift changes of the C2H resonances of histidines as a function of pH in the WT monomer. For His 72 and 68, there is no significant change in the chemical shift at pH < 4.2, but a slight change is observed between 4.2 and 5.3, indicating that these groups begin to deprotonate in the monomer and will have a pK_a significantly >5.3. At pH > 5.3, the monomer peaks disappear, while the dimer peaks gain intensity. The dimer
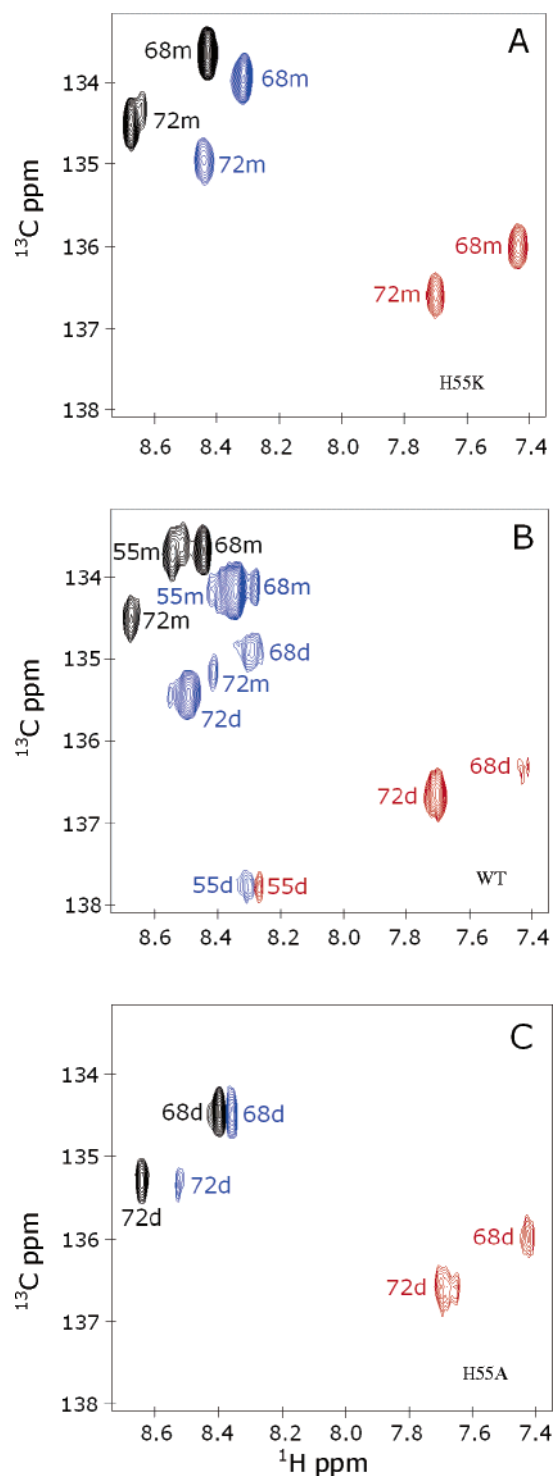
FIGURE 4: ^{13}C CT-HSQC spectra showing the histidine C2H region at pH 3 (black), pH 5 (blue), and pH 7 (red) of (A) H55K, (B) WT-LC8, and (C) H55A. The three histidines are designated as "m" in H55K and the pH-induced WT monomer and "d" in H55A and the WT dimer. The extra peak in the WT that overlaps with 55m is due to residual impurity from the cleaved His tag.

peaks of His 72 and 68 undergo pH titration with a midpoint of 6.1 and 6.0, respectively, close to the value of an unperturbed pK_a (parts B and D of Figure 5).

For His 55, the pH-dependent chemical-shift profile for C2H in the WT monomer, His 55m, is similar to 68 and 72, indicating a pK_a of >5.3. In WT dimer, there is no change in the C2H His 55d chemical shift in the pH range of 4.7–7.7, demonstrating that His 55 in the dimer does not undergo

a pH titration in this pH range. A peak for the dimer first appears at pH 4.7 and increases in intensity as the pH increases, suggesting that at pH 4.7 the dimer is not fully populated (from the population measurements shown below, the dimer is about half-populated at pH 4.7). His 55 titration cannot be monitored completely in the monomer or in the dimer because deprotonation and association are tightly coupled, and therefore, the deprotonated monomer and protonated dimer do not have detectable NMR peaks.

pH Dependence of Monomer and Dimer WT-LC8 Populations. The monomer and dimer populations were determined from the monomer and dimer C2H peak intensities of the three histidine residues (Figure 6). With rising pH, peak intensities of the monomer, measured for His 72 and 68, decrease until no detectable population is observed at pH > 5.3. In the pH range of 4.2–5.3, a peak for the dimer, measured for each histidine C2H, (His 55d starts appearing at pH 4.7) in addition to that of the monomer peak, increases in intensity as the pH increases until it reaches a plateau at pH 7.0. The population curves for the monomer and dimer intersect at pH 4.5, indicating that they all have similar monomer–dimer titration midpoints. Data for His 55d show slightly more scatter partly because of peak broadening. At lower pH, the peaks are completely broadened and invisible in the NMR spectra. A population curve for His 55m is not shown here because of its overlap with the residual impurity peak from the cleaved fusion peptide.

pH Titrations of Monomeric His 55 Mutant. Figure 7 shows pH dependence of His 72 and His 68 chemical shifts in monomeric H55K. Both residues have pH titration curves similar to the corresponding residues in the WT dimer with a pK_a of 6.2 and 6.5, respectively. The pK_a values are within the range expected for an exposed histidine in an unperturbed or random coil environment (*34*) and are slightly higher than those in the dimer, possibly reflecting the increase in solvent accessibility of these residues upon dissociation.

DISCUSSION

Protonation of His 55 and Dimer Dissociation Are Tightly Coupled. Dynein light-chain LC8 is a moderately tight dimer at physiological pH but can exist as a monomer at a low protein concentration ($K_d \sim 12\ \mu M$) or at pH < 4 (*24*). The midpoint of acid-induced dissociation was determined to be 4.8 using molecular weights obtained from sedimentation equilibrium. We have proposed that, upon protonation of the proximate His 55 and His 55′ at the dimer interface, the mutual repulsion of the positive charges, in combination with their increased polarity in a hydrophobic environment, favors dissociation of the dimer. The coupling between the ionization state of His 55 and monomer–dimer equilibrium of LC8 is supported by mutagenesis studies; substitution of His 55 to Lys results in a monomer at pH 7, and a mutation of His 55 to Ala results in a dimer at all pH values studied. To support the role of protonation of His 55 in the dimer dissociation, ^1H and ^{13}C NMR chemical-shift data were obtained for the C2H resonances of each histidine residue. There is a large difference in the chemical shift *between* the monomer and dimer, consistent with deprotonation and burial in the dimer hydrophobic environment. If protonation is coupled to dimer dissociation, then the pK_a of His 55 should be about 4.8 in accordance with the global monomer–dimer titration midpoint determined from sedimentation equilibri-
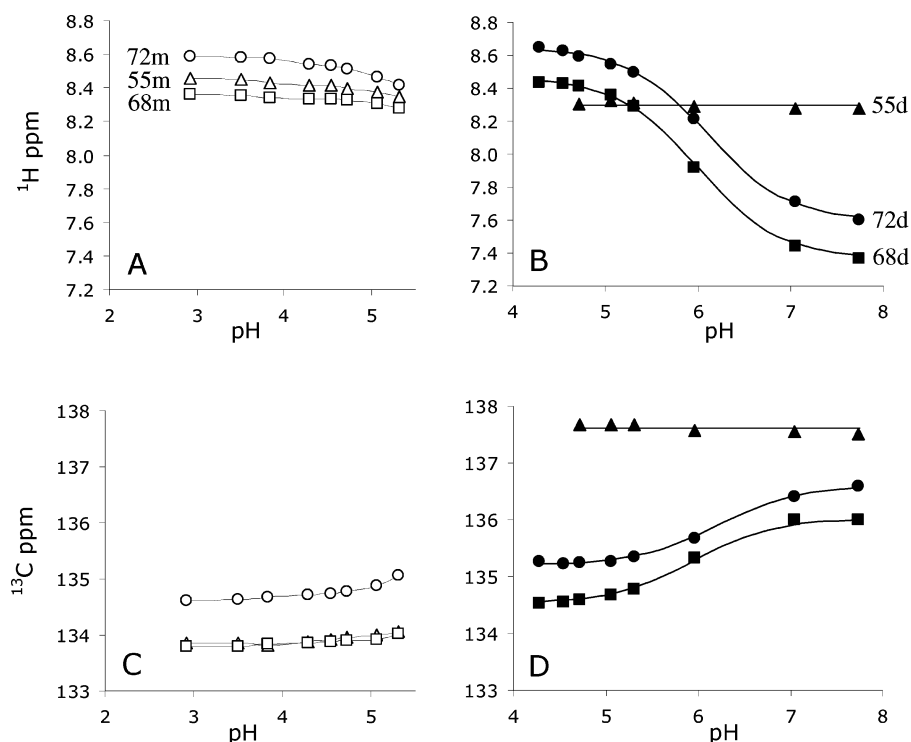
FIGURE 5: pH titration curves of WT-LC8. The proton and carbon chemical shifts as a function of pH are shown for His 72 (○), His 68 (□), and His 55 (△) for the pH-induced monomer (A and C) and for His 72 (●), His 68 (■), and His 55 (▲) for the WT dimer (B and D). The curves for His 68 and 72 dimer (B and D) were obtained by nonlinear least-squares fit of eq 1, and data are shown in Table 1. The lines through the other points are drawn to guide the eye.

Table 1: Summary of pK_a Values of Histidine Residues in WT and Mutant LC8

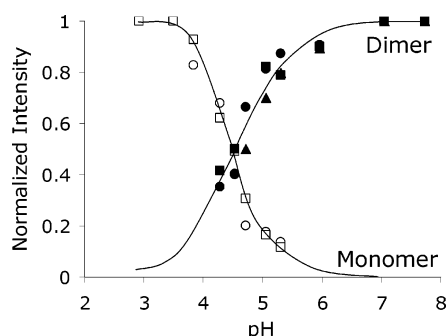| residue	pK_a	
	H55K-LC8	WT-LC8 dimer
His 55		∼4.5
His 68	6.5 ± 0.1	6.0 ± 0.1
His 72	6.2 ± 0.1	6.1 ± 0.1

FIGURE 6: Populations of monomer and dimer WT-LC8 as a function of pH shown for C2H resonances of His 72 (○) and His 68 (□) in the monomer and for C2H resonances of His 72 (●), His 68 (■), and His 55 (▲) in the dimer. Monomer and dimer curves intersect at pH 4.5. The intensities were normalized to an internal reference peak for a solvent-exposed tyrosine in the aromatic CT-HSQC that did not change in intensity as a function of pH or upon association, and the highest intensity for each residue was set to 1. The lines are drawn to guide the eye.
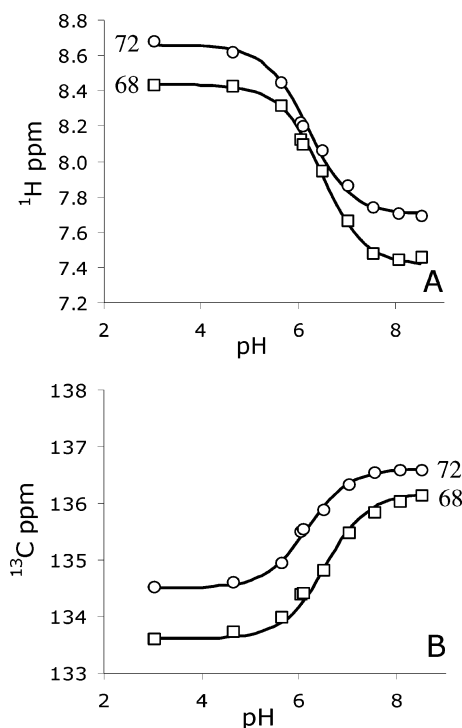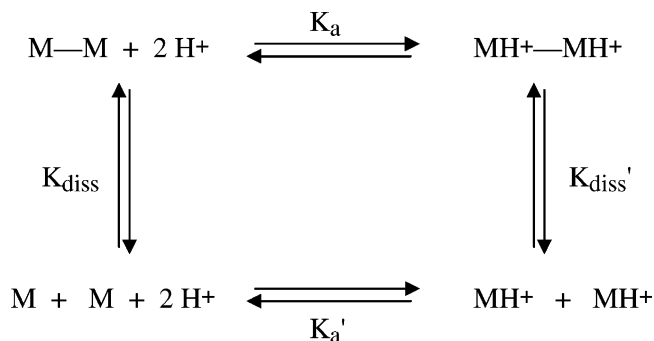

FIGURE 7: pH titration curves of H55K. The proton (A) and carbon (B) chemical shifts are shown for His 72 (○) and His 68 (□). Increase in pH is accompanied by an upfield shift in the proton signal and a downfield shift in the carbon signal. The curves were obtained by nonlinear least-squares fit of eq 1, and data are shown in Table 1.

um. While there is no change in His 55 C2H chemical shifts in the monomer or dimer to allow direct measurement of its pK_a, evidence for a pK_a of about 4.5 in the dimer is based on the following observations: His 55 is in the neutral state in the pH range of 4.7−7.7 and is about 50% populated at

pH 4.7 as measured by peak intensity of C2H peak intensities of His 55d, and the population curves for His residues in the monomer and dimer all have a similar monomer−dimer titration midpoint of pH 4.5.

Linkage between the dissociation and protonation of His 55 requires that, upon protonation of His 55, the LC8 dimer is dissociated. A comparison of size-exclusion profiles and NMR spectra of LC8 at pH 3 and 7 before and after incubation at pH 3 indicates that protonation of His 55 dissociates the dimer and that pH-induced dissociation is reversible, inconsistent with earlier reports of irreversibility (*35*). The reversibility allows for obtaining the thermodynamic parameters in the cycle that represent this linkage

$$
\begin{array}{ccc}
\text{M—M} + 2\,\text{H}^+ & \xrightleftharpoons{K_a} & \text{MH}^+\text{—MH}^+ \\
\Big\updownarrow K_{diss} & & \Big\updownarrow K_{diss}{}' \\
\text{M} + \text{M} + 2\,\text{H}^+ & \xrightarrow{\ \ \ \ \ } & \text{MH}^+ + \text{MH}^+ \\
& K_a{}' &
\end{array}
$$

where M−M and MH$^+$−MH$^+$ correspond to the unprotonated and protonated dimer, respectively, and M and MH$^+$ correspond to the unprotonated and protonated monomer, respectively. K_a and $K_a{}'$ are ionization constants of buried His 55 in the dimer (pK_a of 4.5 and $K_a = 10^{-pK_a}$) and of solvent-exposed His 55 in the monomer (pK_a of 6.5, taken as the unperturbed value), respectively. The pK_a of His 55 in the monomer cannot be measured directly but is likely to be close to 6.5, similar to the pK_a of His 68, which is also solvent-exposed and disordered in the monomer. K_{diss} and $K_{diss}{}'$ are dissociation constants for the unprotonated and protonated dimer, respectively. K_{diss} of 12 μM was measured previously from sedimentation equilibrium at 4 °C. Using this scheme, independent measurements of K_{diss}, K_a, and $K_a{}'$ allow determination of a value for $K_{diss}{}'$ from

$$K_{diss}{}' = K_a K_{diss}/K_a{}'^2$$

to be 3.8×10^3 M, favoring dissociation upon dimer protonation and corresponding to a free energy of −5 kcal/mol (calculated from $\Delta G = -RT \ln K_{diss}$). The free energy for protonation of two monomers is −17.7 kcal/mol, bottom horizontal (calculated from $\Delta G = 2.303RTpK_a{}'$ for each monomer), and is equal to the sum of free energies of dimer association, left vertical (−6.3 kcal/mol), dimer protonation, top horizontal (−6 kcal/mol), and protonated dimer dissociation, right vertical (−5 kcal/mol).

Residues Involved in Intermolecular Hydrogen Bonds. In the crystal structure, Tyr 65 and His 55 form intermolecular hydrogen bonds between phenolic OH of Tyr 65 and Nϵ of Lys 44′ and between His 55 NϵH and C=O of Thr 67′. To explore the roles of these residues in the assembly of the dimer, Tyr 65 was replaced with Phe and Lys and His 55 was replaced with Ala and Lys. Size-exclusion chromatography shows that a substitution of His 55 by Ala and Tyr 65 by Phe or Lys does not detectably change the association state at pH 7. However, replacement of His 55 with Lys, which introduces a positive charge at pH 7, completely dissociates the dimer. The reason that H55K is a monomer, while Y65K remains a dimer, is likely due to the solvent exposure of the tyrosine ring, which has a large molecular

surface area of 60 Å^2 that can accommodate the positive charges, while His 55 is completely buried. In addition, His 55 is stacked within 6 Å against His 55′, and Lys 43 is within 6 Å from His 55 in the same subunit. Protonation of His 55 will therefore result in a change of the environment of the imidazole rings to prevent the highly unfavorable formation of four positive charges in a row (Figure 1C). Therefore, replacement of any interface residue with a positive side chain is not sufficient for dissociation; apparently the geometry, the hydrophobic environment, and the alignment of other charges in the vicinity are also important factors.

Comparison to Other Buried Histidines. The standard pK_a of an imidazole ring is close to physiological pH and allows for the ionization state of this side chain to have an effective regulatory role. Buried histidines have a wide range of pK_a values depending upon multiple environmental contributions, including hydrogen-bond interactions, electrostatic interactions, and solvent inaccessibility (*36*). Buried histidines can have pK_a values as low as 2, but there are exceptions where completely buried histidines have pK_a values close to normal (*37*). Unusually low pK_a values were observed for His 25 in FK506-binding protein and His 54 in cyclophilin, for example, as a result of their highly positively charged environments (*38*). Another example where a buried environment resulted in a low pK_a is in *Bacillus circulans* xylanase. His 149 is buried within its hydrophobic core and is involved in a network of hydrogen bonds and weak aromatic−aromatic interactions resulting in a pK_a < 2.3 (*39*). Protonation of histidine also destabilizes other protein−protein interfaces. For example, protonation of a histidine at the dimer−dimer interface of tetrameric R67 dihydrofolate reductase causes reversible dissociation into inactive dimers (*40*).

In LC8, molecular-accessible surface areas of the three imidazole rings correlate with their pK_a values in the WT dimer. His 55 is completely buried with a pK_a of about 4.5, while His 68 and His 72 rings are somewhat exposed with a pK_a close to 6 (molecular surface areas of 40 Å^2 for each). Proximity to Lys 43 may also contribute to a depressed pK_a for His 55 in the dimer.

Implications for Functional Significance. In functional studies, the active form of LC8 is dimeric; however, the activity of a monomer at physiological pH has not been tested previously. At pH 7, monomeric H55K does not bind the dynein intermediate chain IC74 (Norwood and Barbar, unpublished data), consistent with the expectation that dimerization is necessary for LC8 to be part of the dynein complex. Dimeric H55A still binds IC74, suggesting that binding is not due to the specific interaction with His 55. The *in vivo* significance of the monomer−dimer equilibrium for regulating LC8 assembly with dynein is not clear. It is possible that the local protein concentration may increase the population of monomers and/or that interactions with other proteins or phosphorylation of three-dimensionally proximal residues (*6*) may influence the environment of His 55 to raise its pK_a. The latter could bring the His-55-linked monomer−dimer titration into the physiological pH range.

REFERENCES

1. Vallee, R. B., Williams, J. C., Varma, D., and Barnhart, L. E. (2004) Dynein: An ancient motor protein involved in multiple modes of transport, *J. Neurobiol. 58*, 189−200.

2. Beckwith, S. M., Roghi, C. H., Liu, B., and Morris, N. R. (1998) The 8-kDa cytoplasmic dynein light chain is required for nuclear migration and for heavy chain localization in *Aspergillus nidulans*, *J. Cell Biol. 143*, 1239−1247.

3. Pazour, G. J., Wilkerson, C. G., and Witman, G. B. (1998) A dynein light chain is essential for the retrograde particle movement of intraflagellar transport (IFT), *J. Cell Biol. 141*, 979.

4. Dick, T., Ray, K., Salz, H. K., and Chia, W. (1996) Cytoplasmic dynein (ddlc1) mutations cause morphogenetic defects and apoptotic cell death in *Drosophila melanogaster*, *Mol. Cell. Biol. 16*, 1966−1977.

5. Lo, K. W., Kan, H. M., Chan, L. N., Xu, W. G., Wang, K. P., Wu, Z., Sheng, M., and Zhang, M. (2004) The 8 kDa dynein light chain binds to 53BP1 and mediates DNA damage-induced p53 nuclear accumulation, *J. Biol. Chem.*

6. Vadlamudi, R. K., Bagheri-Yarmand, R., Yang, Z., Balasenthil, S., Nguyen, D., Sahin, A. A., den Hollander, P., and Kumar, R. (2004) Dynein light chain 1, a p21-activated kinase 1-interacting substrate, promotes cancerous phenotypes, *Cancer Cell 5*, 575−585.

7. Espindola, F. S., Suter, D. M., Partata, L. B. E., Cao, T., Wolenski, J. S., Cheney, R. E., King, S. M., and Mooseker, M. S. (2000) The light chain composition of brain Myosin-Va: Calmodulin, myosin-II essential light chains, and 8-kDa dynein light chain/PIN, *Cell Motil. Cytoskeleton 47*, 269−281.

8. Jaffrey, S. R., and Snyder, S. H. (1996) PIN: An associated protein inhibitor of neuronal nitric oxide synthase, *Science 274*, 774−777.

9. Schnorrer, F., Bohmann, K., and Nusslein-Volhard, C. (2000) The molecular motor dynein is involved in targeting Swallow and the bicoid RNA to the anterior pole of *Drosophila* oocytes, *Nat. Cell Biol. 2*, 185−190.

10. Puthalakath, H., Huang, D. C. S., O'Reilly, L. A., King, S. M., and Strasser, A. (1999) The proapoptotic activity of the Bcl-2 family member Bim is regulated by interaction with the dynein motor complex, *Mol. Cell 3*, 287−296.

11. Kaiser, F. J., Tavassoli, K., van den Bemd, G. J., Chang, G. T. G., Horsthemke, B., Moroy, T., and Ludecke, H. J. (2003) Nuclear interaction of the dynein light chain LC8a with the TRPS1 transcription factor suppresses the transcriptional repression activity of TRPS1, *Hum. Mol. Genet. 12*, 1349−1358.

12. Alonso, C., Miskin, J., Hernaez, B., Fernandez-Zapatero, P., Soto, L., Canto, C., Rodriguez-Crespo, I., Dixon, L., and Escribano, J. M. (2001) African swine fever virus protein p54 interacts with the microtubular motor complex through direct binding to light-chain dynein, *J. Virol. 75*, 9819−9827.

13. Raux, H., Flamand, A., and Blondel, D. (2000) Interaction of the rabies virus P protein with the LC8 dynein light chain, *J. Virol. 74*, 10212−10216.

14. Jacob, Y., Badrane, H., Ceccaldi, P. E., and Tordo, N. (2000) Cytoplasmic dynein LC8 interacts with lyssavirus phosphoprotein, *J. Virol. 74*, 10217−10222.

15. Fan, J. S., Zhang, Q., Tochio, H., Li, M., and Zhang, M. J. (2001) Structural basis of diverse sequence-dependent target recognition by the 8 kDa dynein light chain, *J. Mol. Biol. 306*, 97−108.

16. King, S. M. (2000) The dynein microtubule motor, *Biochim. Biophys. Acta 1496*, 60−75.

17. Wu, H., Maciejewski, M. W., Takebe, S., and King, S. M. (2005) Solution structure of the Tctex1 dimer reveals a mechanism for dynein−cargo interactions, *Structure 13*, 213−223.

18. Makokha, M., Hare, M., Li, M. G., Hays, T., and Barbar, E. (2002) Interactions of cytoplasmic dynein light chains Tctex-1 and LC8 with the intermediate chain IC74, *Biochemistry 41*, 4302−4311.

19. Nyarko, A., Hare, M., Makokha, M., and Barbar, E. (2003) Interactions of LC8 with N-terminal segments of the intermediate chain of cytoplasmic dynein, *ScientificWorld J. 3*, 647−658.

20. Nyarko, A., Hare, M., Hays, T. S., and Barbar, E. (2004) The intermediate chain of cytoplasmic dynein is partially disordered and gains structure upon binding to light-chain LC8, *Biochemistry 43*, 15595−15603.

21. Wang, L., Hare, M., Hays, T., and Barbar, E. (2004) Dynein light chain LC8 promotes the assembly of the coiled coil domain of swallow protein, *Biochemistry 43*, 4611−4620.

22. Lo, K. W. H., Naisbitt, S., Fan, J. S., Sheng, M., and Zhang, M. J. (2001) The 8-kDa dynein light chain binds to its targets via a conserved (K/R)XTQT motif, *J. Biol. Chem. 276*, 14059−14066.

23. Liang, J., Jaffrey, S. R., Guo, W., Snyder, S. H., and Clardy, J. (1999) Structure of the PIN/LC8 dimer with a bound peptide, *Nat. Struct. Biol. 6*, 735−740.

24. Barbar, E., Kleinman, B., Imhoff, D., Li, M. G., Hays, T. S., and Hare, M. (2001) Dimerization and folding of LC8, a highly conserved light chain of cytoplasmic dynein, *Biochemistry 40*, 1596−1605.

25. Makokha, M., Huang, Y. J., Montelione, G., Edison, A. S., and Barbar, E. (2004) The solution structure of the pH-induced monomer of dynein light-chain LC8 from *Drosophila*, *Protein Sci. 13*, 727−734.

26. Delaglio, F., Grzesiek, S., Vuister, G. W., Zhu, G., Pfeifer, J., and Bax, A. (1995) NMRPipe—A multidimensional spectral processing system based on unix pipes, *J. Biomol. NMR 6*, 277−293.

27. Johnson, B. A. (2004) Using NMRView to visualize and analyze the NMR spectra of macromolecules, *Methods Mol. Biol. 278*, 313−352.

28. Grzesiek, S., and Bax, A. (1993) Amino acid type determination in the sequential assignment procedure of uniformly $^{13}C/^{15}N$-enriched proteins, *J. Biomol. NMR 3*, 185−204.

29. Song, J., Laskowski, M., Jr., Qasim, M. A., and Markley, J. L. (2003) NMR determination of pK_a values for Asp, Glu, His, and Lys mutants at each variable contiguous enzyme−inhibitor contact position of the turkey ovomucoid third domain, *Biochemistry 42*, 2847−2856.

30. Markley, J. L., Ulrich, E. L., Berg, S. P., and Krogmann, D. W. (1975) Nuclear magnetic resonance studies of the copper binding sites of blue copper proteins: Oxidized, reduced, and apoplastocyanin, *Biochemistry 14*, 4428−4433.

31. Wilson, N. A., Barbar, E., Fuchs, J. A., and Woodward, C. (1995) Aspartic acid 26 in reduced *Escherichia coli* thioredoxin has a $pK_a > 9$, *Biochemistry 34*, 8931−8939.

32. Forsyth, W. R., Gilson, M. K., Antosiewicz, J., Jaren, O. R., and Robertson, A. D. (1998) Theoretical and experimental analysis of ionization equilibria in ovomucoid third domain, *Biochemistry 37*, 8643−8652.

33. Pelton, J. G., Torchia, D. A., Meadow, N. D., and Roseman, S. (1993) Tautomeric states of the active-site histidines of phosphorylated and unphosphorylated IIIGlc, a signal-transducing protein from *Escherichia coli*, using two-dimensional heteronuclear NMR techniques, *Protein Sci. 2*, 543−558.

34. Creighton, T. E. (1993) *Proteins: Structures and Molecular Properties*, 2nd ed., W. H. Freeman and Company, New York.

35. Wang, W., Lo, K. W., Kan, H. M., Fan, J. S., and Zhang, M. (2003) Structure of the monomeric 8-kDa dynein light chain and mechanism of the domain-swapped dimer assembly, *J. Biol. Chem. 278*, 41491−41499.

36. Mehler, E. L., Fuxreiter, M., Simon, I., and Garcia-Moreno, E. B. (2002) The role of hydrophobic microenvironments in modulating pK_a shifts in proteins, *Proteins 48*, 283−292.

37. Edgcomb, S. P., and Murphy, K. P. (2002) Variability in the pK_a of histidine side-chains correlates with burial within proteins, *Proteins 49*, 1−6.

38. Yu, L., and Fesik, S. W. (1994) pH titration of the histidine residues of cyclophilin and FK506 binding protein in the absence and presence of immunosuppressant ligands, *Biochim. Biophys. Acta 1209*, 24−32.

39. Plesniak, L. A., Connelly, G. P., Wakarchuk, W. W., and McIntosh, L. P. (1996) Characterization of a buried neutral histidine residue in *Bacillus circulans* xylanase: NMR assignments, pH titration, and hydrogen exchange, *Protein Sci. 5*, 2319−2328.

40. Nichols, R., Weaver, C. D., Eisenstein, E., Blakley, R. L., Appleman, J., Huang, T. H., Huang, F. Y., and Howell, E. E. (1993) Titration of histidine 62 in R67 dihydrofolate reductase is linked to a tetramer ↔ two-dimer equilibrium, *Biochemistry 32*, 1695−1706.